Equilibration of an Atmosphere by Adiabatic Eddy Fluxes

MALTE JANSEN AND RAFFAELE FERRARI

Massachusetts Institute of Technology, Cambridge, Massachusetts

(Manuscript received 10 January 2013, in final form 11 April 2013)

ABSTRACT

A major question for climate studies is to quantify the role of turbulent eddy fluxes in maintaining the observed atmospheric mean state. Both the equator-to-pole temperature gradient and the static stability of the extratropical atmosphere are set by a balance between these eddy fluxes and the radiative forcing. Much attention has been paid to the adjustment of the isentropic slope, which relates the static stability and the meridional temperature gradient. It is often argued that the extratropical atmosphere always equilibrates such that isentropes leaving the surface in the subtropics reach the tropopause near the poles. However, recent work challenged this argument. This paper revisits scaling arguments for the equilibrated mean state of a dry atmosphere, which results from a balance between the radiative forcing and the along-isentropic eddy heat flux. These arguments predict weak sensitivity of the isentropic slope to changes in the radiative forcing, consistent with previous results. Large changes can, however, be achieved if other external parameters, such as the size and rotation rate of the planet, are varied. The arguments are also extended to predict both the meridional temperature gradient and the static stability independently. This allows a full characterization of the atmospheric mean state as a function of external parameters.

1. Introduction

A major question for climate studies is to understand what maintains the observed atmospheric mean state. What determines the equator-to-pole temperature gradient and what sets the static stability? In the extratropical troposphere the mean state is maintained primarily by a balance between the radiative forcing and the energy fluxes associated with large-scale turbulent eddies. Observations suggest that these eddy fluxes equilibrate the time- and zonal-mean state of the extratropical troposphere such that the temperature contrast between the subtropics and the poles is about the same as the potential temperature contrast between the surface and the tropopause. This implies that isentropes leaving the surface in the subtropics reach the tropopause near the pole, and thus $s \sim H/a$, where s denotes a characteristic isentropic slope, H is the depth scale of the troposphere, and a is the planetary radius.

The mean slope of atmospheric isentropes has received a lot of attention as it bears resemblance to the condition for marginal criticality to baroclinic instability in the two-layer quasigeostrophic (QG) model (e.g., Stone 1978). The criticality to baroclinic instability in this model is described by the parameter $\xi \sim sa/H$. Small criticality parameters, $\xi \ll 1$, denote a state that is stable to baroclinic instability, while large criticality parameters, $\xi \gg 1$, denote a strongly unstable state. The mean state of Earth's extratropical troposphere, where $\xi \approx 1$, thus seems to lie near marginal criticality to baroclinic instability.

There are two lines of argument in the literature on how the large-scale turbulent eddy fluxes set the extratropical mean state. One series of studies have suggested that the observed equilibration to mean states with $\xi \approx 1$ results from a fundamental property of baroclinic flows adjusted by large-scale eddies (e.g., Stone 1978; Schneider 2004). This notion is supported by a series of numerical simulations presented in Schneider (2004) and Schneider and Walker (2006), which show that the atmospheric mean state consistently equilibrates in such a way that $\xi \approx 1$ for a wide range of forcings and parameters.

A second, more recent, series of studies has found that an atmosphere can adjust to states with ξ different from one. Numerical simulations adjust to mean states with a wide range of criticality parameters, if the external forcing and planetary parameters are varied sufficiently (e.g., Zurita-Gotor 2008; Zurita-Gotor and Vallis 2010;

Corresponding author address: Malte Jansen, Massachusetts Institute of Technology, 77 Massachusetts Avenue, 54-1615, Cambridge, MA 02139.
E-mail: mfjansen@mit.edu

DOI: 10.1175/JAS-D-13-013.1

Jansen and Ferrari 2012, hereafter JF12; M. F. Jansen and R. Ferrari 2013, unpublished manuscript, hereafter JF13a). The reasons for the breakdown of the argument of Schneider (2004) were discussed in Jansen and Ferrari (2013; JF13a). Here we follow an argument by Held (2007) and show that the criticality parameter is set by a balance between the radiative forcing and the adiabatic eddy fluxes, which in turn can be closed as proposed in Held and Larichev (1996).

Most previous studies have focused on the criticality parameter, which relates the meridional temperature gradient to the bulk static stability (e.g., Zurita-Gotor 2008; Zurita-Gotor and Vallis 2010; JF12). In practice, however, we are often more interested in both the static stability and the meridional temperature gradient and not only in their ratio.

We will begin by deriving a scaling relation for the criticality parameter, similar to the one discussed in JF12. Given the criticality parameter, and thus the slope of the isentropes, the thermodynamic budget will then be used to derive scaling relations for both the meridional temperature gradient and the static stability. Since the heat fluxes associated with large-scale geostrophic eddies are to first-order adiabatic, the net heating along any isentrope must approximately vanish at equilibrium. This provides the thermodynamic constraint necessary to determine the full thermal structure.

This paper is organized as follows: In section 2, we discuss the setup and some basic results from the numerical simulations, which will be used in this study. In section 3 we discuss scaling laws for the criticality parameter, and test them against the numerical simulations. In section 4, we derive and test scalings for both the horizontal temperature gradient and the static stability. A brief summary and discussion of our results is given in section 5.

2. Numerical simulations

The numerical simulations discussed in this paper are described in detail in JF13a. All simulations use the Massachusetts Institute of Technology (MIT) general circulation model (Marshall et al. 1997) to solve the primitive equations for a Boussinesq fluid. The domain is a Cartesian-coordinate, zonally reentrant channel on a β plane; that is, $f = f_0 + \beta y$, where f is the Coriolis parameter and $\beta = \partial_y f$ is the planetary vorticity gradient. This idealized setup allows us to easily vary f_0 and β separately without changing the size of the domain (on a spherical planet the two are related via the planetary radius $a = f/\beta \tan^{-1}\phi$, at each latitude ϕ). As shown in JF13a, this is an efficient way to greatly vary the criticality parameter of the equilibrated mean state.

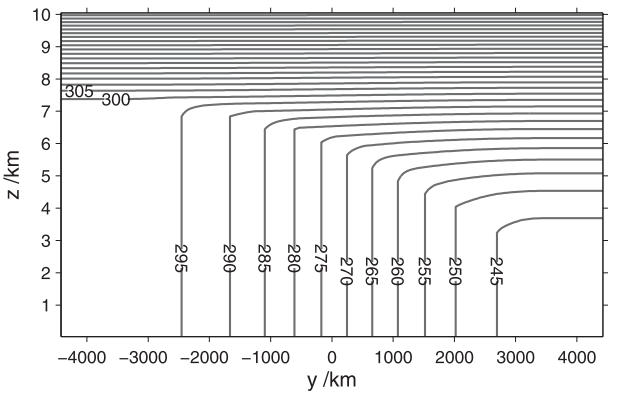

FIG. 1. Equilibrium potential temperature (K) for thermal restoring. Reproduced from JF13a.

The zonally reentrant channel is 15 000 km long, bounded meridionally by sidewalls at $y = \pm 4500$ km, and vertically by a rigid lid at $z = H = 10.2$ km and a flat bottom at $z = 0$. The model resolution is 50 km $\times$ 50 km in the horizontal and uses 29 unevenly spaced levels in the vertical. Free-slip boundary conditions are used on all boundaries, and kinetic energy is removed by a linear Rayleigh drag with a constant drag coefficient of $r = (50 \text{ days})^{-1}$ throughout the domain. We use a linear equation of state: $b = g\alpha(\theta - \theta_0)$, where b is buoyancy, θ_0 is a reference potential temperature, g is the acceleration of gravity, and α is the thermal expansion coefficient. The thermal expansion coefficient used here is chosen to resemble the thermal expansion of air, $\alpha = 3.6 \times 10^{-3}\,\text{K}^{-1}$. Following Held and Suarez (1994), radiative forcing is represented through relaxation to an equilibrium temperature profile, characterized by a baroclinic zone, 7000 km wide, across which the temperature drops by about 55 K. The equilibrium stratification is neutral over the lower part of the domain, while a statically stable equilibrium stratification is prescribed at higher altitudes to mimic the stable radiative equilibrium profile of the stratosphere (Fig. 1). The relaxation time scale is $\tau_s = 14$ days at the surface and decreases exponentially, with an e-folding depth of 500 m, to an interior value of $\tau_{\text{int}} = 50$ days. The simulations are spun up until a quasi-steady state is reached. Diagnostics are calculated over at least 500 days after equilibration is reached, which guarantees that the results presented are not significantly affected by initial transients and high-frequency variability.

A series of 11 simulations is considered, with Coriolis parameters $f_0 = (1, 2, 4, 8) \times 10^{-4}\,\text{s}^{-1}$ and planetary vorticity gradients $\beta = (0.8, 1.6, 3.2) \times 10^{-11}\,\text{m}^{-1}\,\text{s}^{-1}$. All possible combinations of f_0 and β are included, except for $f_0 = 1 \times 10^{-4}\,\text{s}^{-1}$ and $\beta = 3.2 \times 10^{-11}\,\text{m}^{-1}\,\text{s}^{-1}$, for which the Coriolis parameter would change sign within the domain. The largest Coriolis parameter, $f_0 = 8 \times 10^{-4}\,\text{s}^{-1}$, was chosen such that the deformation scale

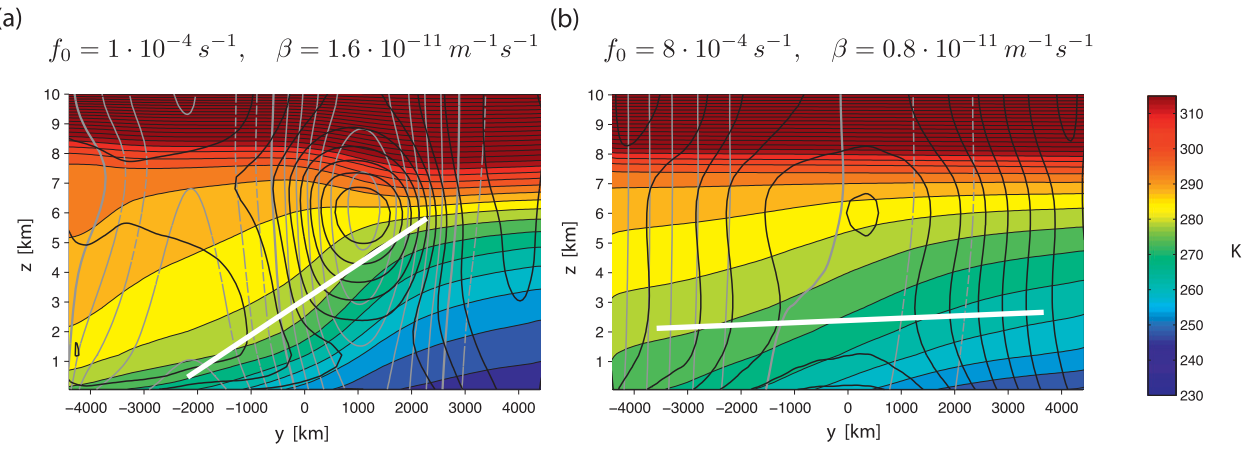

FIG. 2. Time- and zonal-mean cross sections for simulations with (a) $f = 1 \times 10^{-4}\,\mathrm{s}^{-1}$ and $\beta = 1 \times 10^{-11}\,\mathrm{m}^{-1}\,\mathrm{s}^{-1}$ and (b) $f = 8 \times 10^{-4}\,\mathrm{s}^{-1}$ and $\beta = 0.8 \times 10^{-11}\,\mathrm{m}^{-1}\,\mathrm{s}^{-1}$. Colors show potential temperature, gray lines show the zonal wind [contour interval (CI): 5 and 2 m s^{-1} for $f = 1 \times 10^{-4}\,\mathrm{s}^{-1}$ and $\beta = 1 \times 10^{-11}\,\mathrm{m}^{-1}\,\mathrm{s}^{-1}$ and $f = 8 \times 10^{-4}\,\mathrm{s}^{-1}$ and $\beta = 0.8 \times 10^{-11}\,\mathrm{m}^{-1}\,\mathrm{s}^{-1}$, respectively], and thin black lines show EKE (CI: 30 and 10 m^2 s^{-2}, respectively). The thick white lines denote the characteristic isentropic slope expected if $\xi = 1$. The figure is reproduced from JF13a.

(which decreases with increasing f_0) remains well resolved in all simulations, while the smallest planetary vorticity gradient, $\beta = 0.8 \times 10^{-11}\,\mathrm{m}^{-1}\,\mathrm{s}^{-1}$, was chosen such that the Rhines scale (which increases with decreasing β) remains smaller than the size of the domain.

Figure 2 shows the equilibrated time- and zonal-mean state for two illustrative simulations—one using parameters characteristic for Earth's midlatitudes: $f_0 = 1 \times 10^{-4}\,\mathrm{s}^{-1}$ and $\beta = 1.6 \times 10^{-11}\,\mathrm{m}^{-1}\,\mathrm{s}^{-1}$—and one using a much faster rotation rate but less curvature: $f_0 = 8 \times 10^{-4}\,\mathrm{s}^{-1}$ and $\beta = 0.8 \times 10^{-11}\,\mathrm{m}^{-1}\,\mathrm{s}^{-1}$. In the simulation with Earth-like parameters, the channel equilibrates to a state sharing many characteristics with the extratropical atmosphere. In particular, we find $s \sim H/a$, and hence $\xi \approx 1$. Notice that we here define $a \equiv f_0/\beta$, which represents the dynamically relevant length scale that enters into the definition of the criticality parameter: $\xi \equiv (f_0/\beta)s/H$. As in the extratropical atmosphere, the slopes are somewhat steeper in the center of the baroclinic jet than on the flanks.

The simulation with $f_0 = 8 \times 10^{-4}\,\mathrm{s}^{-1}$ and $\beta = 0.8 \times 10^{-11}\,\mathrm{m}^{-1}\,\mathrm{s}^{-1}$, on the other hand, has a criticality parameter much larger than one (Fig. 2b). While the isentropic slope is somewhat flatter than in the Earth-like case (Fig. 2a), the flattening of the isentropic slope does not offset the 16-fold increase of f_0/β. JF13a show that this simulation is also more strongly turbulent, in the sense that there is a significant inverse energy cascade between the deformation scale and the much larger scale of the most energetic eddies.

Supercritical states can also be achieved by strongly reducing the buoyancy gradients in the equilibrium profile (e.g., Zurita-Gotor and Vallis 2010). JF12 find that this is easily achieved by changing only the thermal expansion coefficient α while keeping the temperature radiative equilibrium profile fixed. To further test our theoretical results, we will additionally analyze the simulations of JF12, where α is decreased from atmosphere-like values to ocean-like values. A complete description of the simulations can be found in JF12. The setup is very similar to the one discussed in the beginning of this section. A few differences are, however, worth pointing out. The radiative equilibrium temperature gradient is statically unstable in the lower troposphere, and frictional drag acts only in a viscous surface Ekman layer. None of these differences is crucial for the arguments discussed below. A summary of all simulations used in this manuscript is shown in Table 1.

3. Scaling arguments for the criticality parameter

The simulations described above show that strongly supercritical baroclinic flows can be achieved in primitive equation models by varying f_0 and β. This seems to contradict previous results, which suggested that ξ cannot exceed one in primitive equation models. It is therefore necessary to revisit scaling arguments for the criticality parameter in order to understand how it depends on external parameters, and in particular on f_0 and β.

In this section we derive a scaling argument for the criticality parameter, similar to that proposed in JF12. Instead of using isentropic coordinates, as in JF12, we present a derivation in Cartesian coordinates, which largely follows the arguments by Held (2007) and Zurita-Gotor and Vallis (2009, 2010). The key idea is that the isentropic slope, and thus the criticality parameter, is set through a balance between the radiative forcing and the eddy heat

TABLE 1. Summary of parameters for all simulations appearing in this study. Criticality parameters are computed according to Eq. (10).

Original appearance	f_0 (s^{-1})	β ($m^{-1}s^{-1}$)	α (K^{-1})	ξ
JF13a	1×10^{-4}	1.6×10^{-11}	3.6×10^{-3}	0.96
JF13a	1×10^{-4}	0.8×10^{-11}	3.6×10^{-3}	1.3
JF13a	2×10^{-4}	3.2×10^{-11}	3.6×10^{-3}	1.3
JF13a	2×10^{-4}	1.6×10^{-11}	3.6×10^{-3}	1.6
JF13a	2×10^{-4}	0.8×10^{-11}	3.6×10^{-3}	2.1
JF13a	4×10^{-4}	3.2×10^{-11}	3.6×10^{-3}	2.1
JF13a	4×10^{-4}	1.6×10^{-11}	3.6×10^{-3}	2.7
JF13a	4×10^{-4}	0.8×10^{-11}	3.6×10^{-3}	4.1
JF13a	8×10^{-4}	3.2×10^{-11}	3.6×10^{-3}	4.3
JF13a	8×10^{-4}	1.6×10^{-11}	3.6×10^{-3}	5.9
JF13a	8×10^{-4}	0.8×10^{-11}	3.6×10^{-3}	9.4
JF12	1×10^{-4}	1.6×10^{-11}	1.44×10^{-2}	0.92
JF12	1×10^{-4}	1.6×10^{-11}	7.2×10^{-3}	0.99
JF12	1×10^{-4}	1.6×10^{-11}	3.6×10^{-3}	1.1
JF12	1×10^{-4}	1.6×10^{-11}	1.8×10^{-3}	1.3
JF12	1×10^{-4}	1.6×10^{-11}	0.9×10^{-3}	2.0
JF12	1×10^{-4}	1.6×10^{-11}	4.5×10^{-4}	2.5
JF12	1×10^{-4}	1.6×10^{-11}	2.25×10^{-4}	3.4
JF12	1×10^{-4}	1.6×10^{-11}	1.6×10^{-4}	4.6

flux. In combination with a diffusive scaling argument for the magnitude of the eddy fluxes, this constrains the equilibrated mean state.

All arguments are presented for a Boussinesq fluid with a linear equation of state, as used in the numerical simulations; eddy fluxes and gradients of buoyancy in this case are linearly proportional to eddy fluxes and gradients of potential temperature: $\overline{v'b'} = g\alpha\overline{v'\theta'}$, and $\nabla\overline{b} = g\alpha\nabla\theta$, where overbars denote time and zonal averages, and primes denote deviations thereof. While all equations are expressed in terms of buoyancy, for better readability, we will use the term heat fluxes interchangeably for buoyancy fluxes in the discussions. All results can be easily generalized to an ideal gas if the height coordinate is replaced by pressure.

a. Relating the criticality parameter to the eddy diffusivity

The zonal momentum budget and the thermodynamic equation are now used to derive a relation between the criticality parameter, the radiative forcing, and the eddy diffusivity. Using the QG approximation, and ignoring frictional forces, the zonal momentum budget can be written as (e.g., Vallis 2006)

$$f_0\overline{v}^\dagger = -\overline{v'q'}, \tag{1}$$

where $\overline{v}^\dagger = -\partial_z\Psi^\dagger$ is the residual meridional velocity, with $\Psi^\dagger = -\int_0^z \overline{v}\,dz' + \overline{v'b'}/\partial_z b_0$ denoting the residual overturning streamfunction, $\partial_z b_0$ is the background stratification, $q \approx f_0 + \beta y + \zeta + f_0\partial_z(b/\partial_z b_0)$ is the QG potential vorticity (PV), and $\zeta = \partial_x v - \partial_y u$ is the relative vorticity.

Vertically integrating Eq. (1) from the surface yields an equation for the residual overturning streamfunction:

$$\Psi^\dagger = f_0^{-1}\int_0^z \overline{v'q'}\,dz' + \frac{\overline{v'b'}^s}{\partial_z b_0(0)}, \tag{2}$$

where $\overline{(\cdot)}^s$ denotes an average along the surface at $z = 0$. The total mass transport below some level z is thus given by the sum of a contribution associated with the eddy flux of PV in the interior and a contribution associated with the eddy flux of buoyancy at the surface.

As in JF12, we assume that the eddy PV flux and the surface buoyancy flux can be expressed in terms of downgradient flux closures; that is, $\overline{v'q'} = -D\partial_y\overline{q}$ and $\overline{v'b'}^s = -D_s\partial_y\overline{b}^s$. We further focus on the strongly supercritical limit; that is, $\xi \gg 1$. As shown in JF13a, eddies then become strongly barotropic and the eddy diffusivity becomes approximately constant in the vertical. Moreover, the eddy PV diffusivity D is similar to the eddy diffusivity of surface buoyancy D_s, as expected if eddies stir tracer contours independent of the tracer under consideration. Equation (2) then becomes

$$\Psi^\dagger \approx D(s - \beta/f_0 z), \tag{3}$$

where $s = -\partial_y\overline{b}/\partial_z b_0$ is the isentropic slope at z, and we neglected contributions to the PV gradient from the relative vorticity of the mean flow. For $z < H$, where H is the height of the tropopause, and $\xi \sim f_0 s/(\beta H) \gg 1$, the second term on the rhs of Eq. (3) is negligible and we are left with

$$\Psi^\dagger \approx Ds. \tag{4}$$

For marginally critical mean states, where the planetary vorticity gradient β modifies the PV gradient significantly, and the PV diffusivity has strong vertical structure, the physical underpinning of Eq. (4) is less clear.[1]

[1] Equation (4) is commonly used to parameterize the eddy-driven overturning circulation in ocean models (Gent and McWilliams 1990). It is typically motivated in terms of a closure for the horizontal eddy buoyancy flux $\overline{v'b'} = -D\partial_y\overline{b}$ at every vertical level. Using this closure, Eq. (4) can be derived without the assumption of a supercritical mean state. This derivation is also used in Held (2007) and Zurita-Gotor and Vallis (2009, 2010). We here used a derivation based on a downgradient closure for the horizontal eddy QG PV flux. This is more easily defended, since QG PV is conserved following horizontal motion, and hence tends to be mixed in horizontal planes. Buoyancy, instead, is not conserved along horizontal planes away from the surface, because buoyancy perturbations b' can also be generated by vertical velocities acting on the background stratification, $\partial_z\overline{b}_0$. Hence the assumption that the horizontal buoyancy flux is only proportional to the horizontal mean gradient is hard to defend in general. Gent et al. (1995) invoked global energetic arguments to defend the downgradient closure for buoyancy, but it is not clear why global arguments should imply local downgradient fluxes.

The empirical results presented below, however, support the use of Eq. (4) even in this limit.

We now derive a second relation for $\Psi^\dagger$ from the thermodynamic budget. Together with Eq. (4), this will allow us to derive an expression for the criticality parameter as a function of the diabatic forcing and the eddy diffusivity. While the momentum budget for the planetary-scale atmospheric circulation is well described by the QG approximation, the thermodynamic budget cannot be described adequately using the QG equations (e.g., JF12). We will therefore use the thermodynamic budget for the full primitive equations.

Following the argument of Held (2007), we assume that the eddies are approximately adiabatic, and thus eddy heat fluxes are directed primarily along isentropes. Hence the eddy fluxes move mean buoyancy around but do not mix it across isentropes. Their effect is then captured entirely by their contribution to the residual streamfunction—additional terms would imply a cross-isentrope component (e.g., Plumb and Ferrari 2005). The time- and zonal-mean buoyancy budget thus reduces to a balance between the advection by the residual overturning circulation and the mean diabatic forcing:

$$J(\Psi^\dagger, \overline{b}) \approx \overline{\dot{b}}, \tag{5}$$

where $J(A, B) = \partial_y A \partial_z B - \partial_z A \partial_y B$ denotes the Jacobian in the y–z plane, and $\dot{b}$ denotes the diabatic (radiative) forcing.

Choosing a level z_1, that separates net warming (below) and net cooling (above), the heat transport across this level needs to balance the cooling above it. Integrating horizontally, we find that

$$-\Psi^\dagger(y_1, z_1) L \partial_y \overline{b} \sim QHL, \tag{6}$$

where $\Psi^\dagger(y_1, z_1)$ denotes the maximum residual overturning transport across the level z_1. $L\partial_y\overline{b}$ denotes the buoyancy difference between the upwelling and downwelling branches of the eddy-driven overturning circulation, $Q = -(1/HL)\int_{z_1}^{z_t}\int_{y_{\min}}^{y_{\max}} \overline{\dot{b}}\, dy\, dz$ denotes the average radiative cooling in the upper troposphere, and $H = z_t - z_1$ is the depth scale of the upper troposphere. In practice, cooling typically dominates over more than half of the troposphere, and we may, for scaling purposes, assume that H is of the same order as the total depth of the troposphere. This assumption may not be appropriate when considering the response to changes in the vertical structure of the radiative forcing because the vertical extent of the levels of net warming and cooling may change independently from the tropopause height. Changes in the vertical structure of the radiative forcing are not explored systematically in this study. The term $\Psi^\dagger(y_1, z_1)$ will be approximated by the global maximum of the overturning transport because cooling above z_1 is balanced by warm air advection from lower latitudes, while heating below z_1 is balanced by cold-air advection from higher latitudes. The meridional advection thus changes sign near z_1, implying a maximum in the residual overturning at this level[2] (see sketch in Fig. 3).

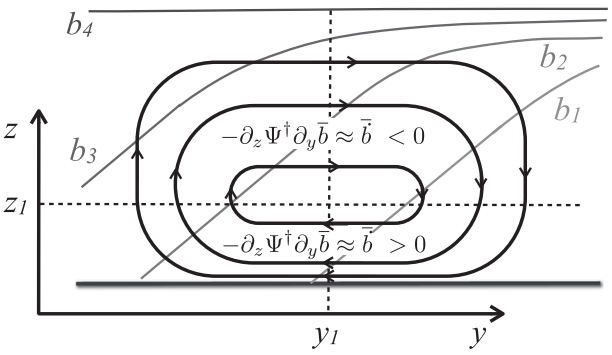

FIG. 3. Schematic indicating the relation between y_1, z_1, and $\Psi^\dagger$ (see text).

The radiative forcing in our simulations is described as a restoring to a radiative equilibrium buoyancy $b_{\rm eq}$ over a time-scale τ, $\dot{b} = -(b - b_{\rm eq})/\tau$. This is a common way to parameterize the effects of radiative heating in idealized models (e.g., Held and Suarez 1994). The average diabatic cooling in the upper troposphere then scales as

$$Q \sim \frac{(\partial_z \overline{b} - \partial_z b_{\rm eq})H}{\tau}. \tag{7}$$

To simplify the algebra we assume that the troposphere is restored toward a statically neutral state, $\partial_z b_{\rm eq} = 0$, but it is straightforward, if tedious, to extend the analysis to $\partial_z b_{\rm eq} \neq 0$. Combining Eqs. (4), (6), and (7) then yields

$$s \sim \frac{H}{\sqrt{\tau D}}. \tag{8}$$

[2] Notice that z_1 denotes the level that separates net warming and cooling in the global mean. Locally at the latitude y_1, the change in sign of the diabatic forcing may occur at a slightly different level, implying that $\Psi^\dagger(y_1, z_1)$ is not exactly the global maximum of $\Psi^\dagger$. Moreover, the representation of the heat transport by a residual overturning streamfunction in z coordinates is justified strictly only in the limit of nearly adiabatic, small-amplitude eddies (e.g., Plumb and Ferrari 2005). These approximations are adequate for the bulk scaling relations derived below but may require further consideration when deriving local arguments or when considering strongly inhomogeneous domains. A more general derivation, using isentropic coordinates, is presented in JF12.

Equation (8) states that the length of an isentrope from the surface to the tropopause, $l_{\text{isen}} \sim \text{s}^{-1}H$, scales with $l_{\text{diff}} \sim \sqrt{\tau D}$—the distance over which eddies mix a tracer on the time scale of the radiative restoring τ.

Equation (8) can easily be transformed into a scaling relation for the criticality parameter. Using that $\xi \sim sa/H$ we obtain that

$$\xi \sim \frac{a}{\sqrt{\tau D}}. \tag{9}$$

Thus, the criticality parameter scales as the ratio of the planetary scale, $a \equiv f_0/\beta$, to the diffusive length scale, $l_{\text{diff}} \sim \sqrt{\tau D}$. Equation (9) suggests that eddies can maintain mean states with $\xi \lesssim 1$ only if $l_{\text{diff}} \gtrsim a$ (i.e., if they can effectively homogenize PV gradients over a scale similar or larger than the planetary scale, on the time scale of the radiative restoring). If instead $l_{\text{diff}} \ll a$—that is, if eddies homogenize PV gradients only over a scale much smaller than the planetary scale on the time scale of the radiative restoring—strongly supercritical mean states are expected.

b. Comparison to numerical results

Before proceeding to relate the eddy diffusivity to the mean state itself, we test the scaling relation in Eq. (9) against the numerical simulations with varying f_0 and β. Similar scaling relations have been used in JF12 to explain changes in the criticality parameter in their simulations with varying thermal expansion coefficient. We estimate criticality parameters for all simulations as in JF13a:

$$\xi \equiv \frac{f_0/\beta \langle \partial_y \overline{b} \rangle}{H \langle \partial_z \overline{b} \rangle}, \tag{10}$$

where the angle brackets denote a horizontal average, taken over the baroclinically forced region between $-3500 < y < 3500$ km, at the fixed level $z = 2$ km, which approximately corresponds to the level z_1 that separates net cooling (above) and warming (below). As discussed by Held (1982) and Zurita-Gotor and Vallis (2011), the tropopause height H is constrained by a "matching condition" between the dynamically controlled tropospheric temperature profile and the radiative equilibrium temperature profile above. Because the radiative equilibrium temperature increases very sharply in the upper part of our domain, changes in the tropopause height are negligible even if the tropospheric static stability changes significantly. For simplicity we thus set $H = 7$ km in Eq. (10) for all simulations. Consistent with the discussion in section 2, Table 1 shows that the criticality parameter varies by about an order of magnitude over the simulations, ranging from about $\xi \approx 1$ for the simulation with Earth-like rotational parameters, $f_0 = 1 \times 10^{-4}\,\text{s}^{-1}$ and $\beta = 1.6 \times 10^{-11}\,\text{m}^{-1}\,\text{s}^{-1}$, to about $\xi \approx 10$ for the simulation with $f_0 = 8 \times 10^{-4}\,\text{s}^{-1}$ and $\beta = 0.8 \times 10^{-11}\,\text{m}^{-1}\,\text{s}^{-1}$.

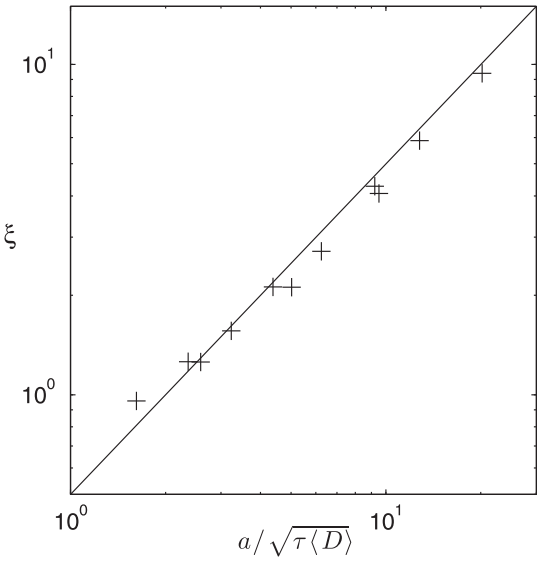

FIG. 4. Criticality parameter against the scaling in Eq. (9), for simulations with various combinations of $f = (1, 2, 4, 8) \times 10^{-4}\,\text{s}^{-1}$ and $\beta = (0.8, 1.6, 3.2) \times 10^{-11}\,\text{m}^{-1}\,\text{s}^{-1}$. The black line shows $\xi = 0.5a/\sqrt{\tau\langle D\rangle}$. The parameter ξ is calculated as in Eq. (10), and $\langle D\rangle$ is calculated as in Eq. (11) and averaged over the width of the baroclinically forced region between $-3500 < y < 3500$ km.

Eddy diffusivities are estimated from a flux–gradient relationship for buoyancy, evaluated at the surface:

$$D = -\frac{\overline{v_s' b_s'}}{\partial_y \overline{b}_s}. \tag{11}$$

The subscript s denotes quantities evaluated at the lowest model level. This diffusivity is similar to the PV diffusivity on isentropes near the surface (JF13a; Jansen and Ferrari 2013).

The scaling relation in Eq. (9) is tested in Fig. 4. We find that it successfully reproduces the domain-averaged criticality parameter of the equilibrated mean state over the whole range of simulations. Next, a closed scaling relation for the equilibrated mean state is obtained by expressing D in terms of the mean state and external parameters.

c. A scaling relation for the criticality parameter

Held and Larichev (1996) proposed an expression for the eddy diffusivity, which has proven useful in previous

studies (e.g., Zurita-Gotor and Vallis 2010; JF12). They argued that eddies in strongly supercritical flows become dominantly barotropic and the eddy mixing length becomes proportional to the Rhines scale $L_\beta \sim \sqrt{V/\beta}$, where V denotes a characteristic barotropic eddy velocity. They further showed that $L_\beta \sim \xi L_d$, where $L_d \sim \partial_z b_0^{1/2} H/f$ is the Rossby radius of deformation. The eddy diffusivity then scales as

$$D \sim L_\beta V \sim \beta L_\beta^3 \sim \beta \xi^3 L_d^3. \tag{12}$$

While the argument was formally derived assuming $\xi \gg 1$, Held and Larichev (1996) show that it reduces to the result of Held (1978) for linear Charney modes in the marginally critical limit. It may thus be expected to hold for both large and $O(1)$ criticality parameters.

Interestingly, the scaling for D in Eq. (12) does not depend on the Coriolis parameter f. While ξ is proportional to f, L_d is proportional to f^{-1}. Thus, D is not directly dependent on changes in f. Together with Eq. (8), this implies that the isentropic slope, but not the criticality parameter, is insensitive to changes in f. We will return to this result in section 3d.

Inserting Eq. (12) into Eq. (9) yields a scaling for the criticality parameter:

$$\xi \sim (f\tau)^{-1/5} \left(\frac{L_d}{a}\right)^{-3/5}. \tag{13}$$

Equation (13) is a specialized version of the scaling relation in Eq. (32) of JF12, for the case in which restoring acts to a statically neutral mean state.[3] The equation predicts that the criticality parameter decreases with an increasing deformation scale normalized by the planetary scale, L_d/a, and it is weakly dependent on the restoring time scale, normalized by the Coriolis parameter, τf.

Equation (13) suggests that typical dry numerical simulations of atmospheres on a full sphere inevitably produce mean states with $O(1)$ criticality parameters. Since the ratio between the restoring time scale and the Coriolis parameter appears with a power of 1/5 in Eq. (13), a tenfold increase in the criticality would require a five-orders-of-magnitude decrease in τf—well outside the range typically explored in simulations of planetary atmospheres. Variations in the normalized deformation scale are easier to achieve in theory, but in global models are limited by numerical constraints: The deformation scale must be significantly smaller than the scale of the planet and well resolved by the numerical grid scale. With a typical horizontal resolution of 1°, this allows for at most one order of magnitude in variations of L_d/a, thus allowing for variations in ξ only up to about a factor of 4.

A similar constraint on the feasible range of values for L_d/a does not hold in our β-plane channel model, where the dynamical planetary-scale $a \equiv f/\beta$ is increased without increasing the size of the domain. We can thus easily set up simulations with $L_d/a \ll 1$ without requiring prohibitive computational resources. Notice, however, that we do not decrease a below the width of the channel to avoid changes in the sign of f, which would introduce spurious equatorial dynamics. If the deformation scale is required to be smaller than the domain size, we are thus still restricted to $L_d/a < 1$. Criticality parameters much smaller than one can therefore only be obtained if τf is increased by many orders of magnitude.

d. Comparison to numerical results

Figure 5 shows that the criticality parameter estimated from the numerical simulations, follows the scaling relation in Eq. (13). Variations in ξ are dominated by changes in the normalized deformation-scale. As f_0 is increased, the deformation scale is reduced, while the dynamical planetary-scale $a \equiv f_0/\beta$ is increased. The normalized deformation scale thus decreases strongly as f is increased. A reduction of the planetary vorticity gradient further reduces the normalized deformation scale by increasing a.

To isolate the dependence of the criticality parameter on the externally prescribed parameters f_0 and β, it is instructive to plug the expression for L_d into Eq. (13), which yields

$$\xi \sim (\tau^2 H^6 \partial_z b_0^3)^{-1/10} \frac{f_0}{\beta^{3/5}}. \tag{14}$$

In the simulations, the prefactor, $(\tau^2 H^6 \partial_z b^3)^{-1/10}$, varies much less than f_0 and β. Consistently, Fig. 4 shows that the criticality parameter scales to leading order as $\xi \propto f_0 \beta^{-3/5}$. As indicated above, ξ is linearly dependent on f_0, implying that the isentropic slope is independent on

[3] The derivation of Eq. (32) in JF12 assumes that the upper-level radiative cooling scales as $Q \sim \tau^{-1}\Delta\theta_{\rm eq}$, where $\Delta\theta_{\rm eq}$ denotes the variation of the radiative equilibrium potential temperature along an isentrope. Owing to the neutral restoring profile used in this study, we have that, in a domain-averaged sense, $Q \sim \tau^{-1}\partial_z\theta H$. Equation (9) is thus recovered by replacing $\Delta\theta_{\rm eq}$ in Eq. (32) of JF12 with $H\partial_z\theta$.

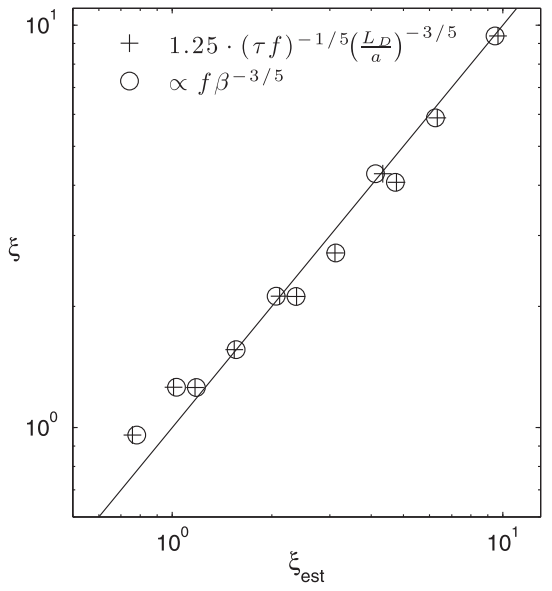

FIG. 5. Criticality parameter against the estimate from the scaling in Eq. (13), for simulations with various combinations of f and β (plus signs). Circles indicate the estimated variations in ξ due to only the direct dependence on f and β [see Eq. (14)]. In both cases, the proportionality constant was chosen to match the data.

f_0—a direct consequence of the eddy diffusivity being independent of f_0, according to the scaling in Eq. (12).

Notice, however, that changes in f_0 strongly affect the characteristics of the flow, even though they only weakly modify the eddy diffusivity and the thermal mean state. The reason is that as f_0 increases, the deformation scale decreases strongly. The eddy kinetic energy and, thus, the Rhines scale, however, remain approximately constant. In agreement with the increasing criticality parameter, we thus observe an increase in the inverse energy cascade range between the deformation scale and the Rhines scale (Held and Larichev 1996). The change in the turbulent flow characteristics of the simulations is analyzed in detail in JF13a.

e. The role of frictional drag

The scaling arguments discussed in this section employ Held and Larichev's (1996) scaling relation for the eddy diffusivity. The derivation of this relation relies on the implicit assumption that the frictional drag acting on the eddies is small. This in turn requires that the majority of the kinetic energy is dissipated by drag on the mean flow.

Thompson and Young (2007) recently questioned the relation proposed by Held and Larichev (1996) showing that frictional drag can strongly affect the eddy diffusivity. Thompson and Young (2007) analyzed a series of numerical simulations using a two-layer QG model with linear drag in the lower layer. They found that the scaling relation proposed by Held and Larichev (1996)[4] provides a reasonable fit to their simulations only in the limit of large criticality parameters and weak frictional drag. In particular, frictional drag becomes important if the frictional spindown time scale τ_{fric} is similar or smaller than the Eady time scale $\tau_E \equiv L_d/U$, where U denotes the vertical shear velocity of the mean flow. With typical atmospheric scales $L_d \sim 1000$ km and $U \sim 10\,\text{m s}^{-1}$, our simulations have Eady time scales on the order of $\tau_E \sim 10^5\,\text{s} \sim 1$ day. The frictional spindown time scale instead is $\tau_{\text{fric}} \approx 50$ days.[5] While τ_E varies across the simulations, it generally stays below about 5 days and, thus, an order of magnitude smaller than the frictional time scale [see Jansen (2012) for a more detailed comparison between our simulations and those of Thompson and Young (2007)].

The limit of strong frictional drag discussed by Thompson and Young (2007) thus appears not to be relevant to the simulations in this study, nor does it seem likely to apply to Earth's atmosphere. Nevertheless, it is important to note that the scaling relations derived here hold only in the limit of small friction and are likely to break down in the presence of strong friction. This limit is probably relevant for eddies in the ocean, where the inverse eddy kinetic energy (EKE) cascade may be strongly modified by frictional drag.

f. Implications for the sensitivity to changes in thermal forcing

We have shown that the criticality parameter can take on a wide range of values if external parameters are varied—a result that may appear inconsistent with previous studies that reported a weak dependence of the criticality parameter to changes in the forcing. In particular, Schneider (2004) and Schneider and Walker

[4] Thompson and Young (2007) compare their results to the scaling relation of Lapeyre and Held (2003), which attempts to generalize the results of Held and Larichev (1996) to the marginally critical limit in the two-layer model. Owing to the large difference between the behavior of the two-layer model and our continuously stratified model near marginal criticality, we here focus our comparison only on the strongly supercritical limit, where the scaling relation in Lapeyre and Held (2003) reduces to the one in Held and Larichev (1996).

[5] Notice that for the simulations with varying f and β, $\tau_{\text{fric}} = 50$ days was prescribed directly as an external parameter. For the simulations with varying thermal expansion coefficient of JF12, the frictional spindown time scale can be estimated from the vertical viscosity, which together with the no-slip bottom boundary condition generates a linear Ekman layer. As for the simulations with varying f and β, the frictional spindown time scale for the barotropic mode is found to be about 50 days (see Jansen 2012).

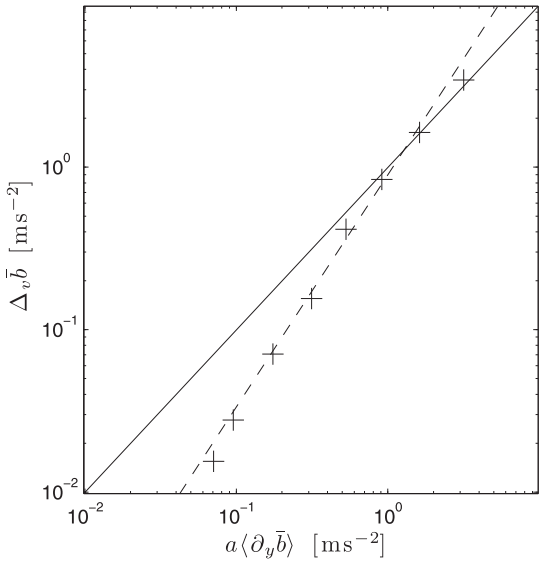

FIG. 6. Bulk static stability against the rescaled horizontal buoyancy gradient for the simulations in JF12, with varying thermal expansion coefficients. The solid line indicates $\Delta_v \bar{b} = a\langle \partial_y \bar{b} \rangle$. The dashed line denotes $\Delta_v \bar{b} \propto (a\langle \partial_y \bar{b} \rangle)^{10/7}$.

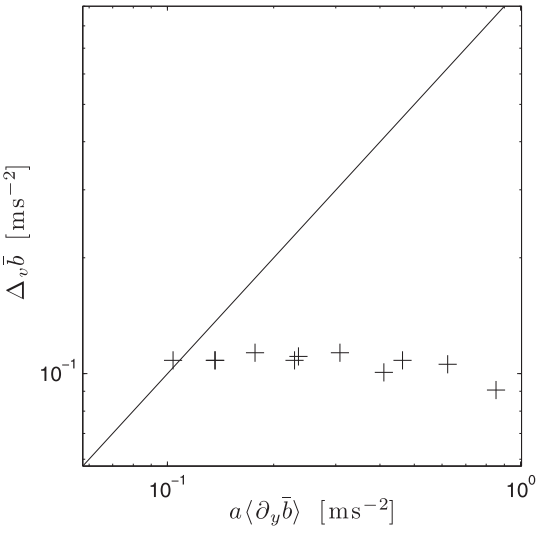

FIG. 7. As Fig. 6, but for the series of simulations with varying f and β.

(2006) analyzed a series of simulations where they varied by large amounts the equator-to-pole temperature gradient in radiative equilibrium. They observed that both the rescaled meridional temperature gradient $a\langle \partial_y \bar{\theta} \rangle$ and the bulk static stability $H\langle \partial_z \bar{\theta} \rangle$ changed strongly across simulations, but their ratio—the criticality parameter—stayed close to one.

A similar result holds for the simulations of JF12. They used a Boussinesq fluid with a linear equation of state $b = \alpha g(\theta - \theta_0)$. They varied α by about two orders of magnitude, spanning from values larger than those found in Earth's atmosphere to values typical for ocean water. Since the radiative equilibrium potential temperature was held constant throughout all simulations, changes in the thermal expansion coefficient directly translated into changes in the radiative equilibrium buoyancy contrasts (both vertical and horizontal). Figure 6 shows the rescaled horizontal buoyancy gradient $a\langle \partial_y \bar{b} \rangle$ against the bulk static stability $\Delta_v \bar{b} \equiv H\langle \partial_z \bar{b} \rangle$ for the series of simulations discussed in JF12. Averages are taken as discussed in section 3b. We observe a large cancellation between changes in the horizontal buoyancy gradient and the bulk static stability, leading to only moderate changes in the criticality parameter. While JF12 report a significant change in the criticality parameter, by about a factor of 4, this must be compared to the two-orders-of-magnitude changes in the buoyancy gradients.

The weak variations in the criticality parameter, compared to the large changes in the meridional buoyancy gradient and static stability, can be understood in terms of the scaling in Eq. (14). Consider the set of simulations of JF12, shown in Fig. 6 and summarized in Table 1; f_0, β, and τ are held constant, and changes in H are negligible compared to those in the buoyancy gradient and static stability. Under these conditions the expression in Eq. (14) gives a relationship between $\Delta_v \bar{b}$ and $a\langle \partial_y \bar{b} \rangle$. Using that $\xi \sim a\langle \partial_y \bar{b} \rangle / \Delta_v \bar{b}$ and $L_d \propto \Delta_v b^{-1/2}$, rearrangement of Eq. (14) yields

$$\Delta_v \bar{b} \propto (a\langle \partial_y \bar{b} \rangle)^{10/7}. \tag{15}$$

Equation (15), which was first derived by Held (2007), predicts that any change in the horizontal buoyancy gradient is associated with a similar, but somewhat larger, change in the bulk static stability. Figure 6 shows that Eq. (15) successfully predicts the relation between the bulk static stability and the meridional buoyancy gradient in the simulations of JF12. A more detailed discussion of the dependence of the criticality parameter to changes in the forcing, for a wide variety of thermal forcing characteristics, is given by Zurita-Gotor and Vallis (2010).

The result in Eq. (15), however, holds solely if the radiative equilibrium buoyancy contrast is the only parameter being changed. The strong cancellation between changes in the rescaled meridional buoyancy gradient and bulk static stability, and thus the weak sensitivity of the criticality parameter, does not hold for other parameter variations. Figure 7 shows that there is no cancellation between changes in the bulk static stability and the rescaled horizontal buoyancy gradient for the series of simulations with varying f_0 and β. While the rescaled horizontal buoyancy gradient varies by about

an order of magnitude, the bulk static stability is rather insensitive to changes in f_0 and β. We return to this result in the next section.

4. The meridional temperature gradient and static stability

Much of the work in this and previous studies (e.g., Stone 1978; Schneider 2004; Zurita-Gotor 2008; Zurita-Gotor and Vallis 2010; JF12) focused on the criticality parameter, which relates the meridional temperature gradient and the bulk static stability. However, for practical purposes, we are interested in both the static stability and meridional temperature gradient separately—not just their ratio. In this section, we extend the scaling laws discussed above to predict both quantities independently.

a. Theory

We here derive constraints for the horizontal buoyancy gradient and bulk static stability. Following the argument in section 3, we assume that the eddy fluxes are adiabatic, such that the heat transport can be expressed in terms of a residual overturning circulation. As discussed in section 3, the vertical heat transport by this residual overturning circulation has to compensate the imbalance in the radiative forcing between the lower and upper troposphere. If the radiative forcing can be expressed in terms of a restoring condition, we can insert Eq. (7) into Eq. (6), which yields

$$-\Psi^{\dagger}(y_1, z_1)\partial_y \overline{b} \sim \frac{(\partial_z \overline{b} - \partial_z b_{\mathrm{eq}})H^2}{\tau}, \tag{16}$$

where $\Psi^{\dagger}(y_1, z_1)$ denotes the maximum residual overturning circulation.

Similarly, the northward heat transport by the residual overturning circulation has to compensate the imbalance in the radiative forcing between the southern and northern part of the domain. Following the same argument as for the derivation of Eq. (16), we obtain

$$\Psi^{\dagger}(y_1, z_1)\partial_z \overline{b} \sim \frac{(\partial_y \overline{b} - \partial_y b_{\mathrm{eq}})L^2}{\tau}. \tag{17}$$

We can eliminate the residual overturning streamfunction by combining Eqs. (16) and (17), which yields

$$-\partial_y \overline{b}(\partial_y \overline{b} - \partial_y b_{\mathrm{eq}})L^2 \sim \partial_z \overline{b}(\partial_z \overline{b} - \partial_z b_{\mathrm{eq}})H^2. \tag{18}$$

Using the definition of the bulk static stability from section 3f, $\Delta_v \overline{b} \equiv H\langle \partial_z \overline{b} \rangle$, and defining an analogous horizontal buoyancy contrast, $\Delta_h \overline{b} \equiv -L\langle \partial_y \overline{b} \rangle$, as well as the corresponding radiative equilibrium values, $\Delta_v b_{\mathrm{eq}}$ and $\Delta_h b_{\mathrm{eq}}$, Eq. (18) predicts that

$$-\Delta_h \overline{b}(\Delta_h \overline{b} - \Delta_h b_{\mathrm{eq}}) \approx \Delta_v \overline{b}(\Delta_v \overline{b} - \Delta_v b_{\mathrm{eq}}). \tag{19}$$

Equation (18) is a scaling relation, which is expected to hold to within an $O(1)$ constant. Instead of explicitly including a constant prefactor in Eq. (19), we absorbed the latter into the length scale L, which enters into the definition of $\Delta_h \overline{b}$ and $\Delta_h b_{\mathrm{eq}}$. The length scale is the width of the baroclinic zone, which is defined up to an $O(1)$ constant. Empirically, we find below that this constant is close to one.

As in section 3, we make the simplifying assumption that the forcing can be approximated by a restoring acting toward an equilibrium buoyancy profile that is statically neutral in the troposphere (i.e., $\partial_z b_{\mathrm{eq}} = 0$). This assumption simplifies the algebra, but it can easily be relaxed. The full case, allowing for nonzero $\partial_z b_{\mathrm{eq}}$ is discussed in appendix A.

Rearrangement of Eq. (19) then yields

$$\Delta_h \overline{b} \approx \frac{\Delta_h b_{\mathrm{eq}}}{1 + \hat{s}^{-2}}, \tag{20}$$

where $\hat{s} \equiv \Delta_h \overline{b}/\Delta_v \overline{b} \sim sL/H$ is the isentropic slope, normalized by the aspect ratio of the baroclinic domain. Equation (20) shows that $\Delta_h \overline{b}$ can be expressed as a function of its radiative equilibrium value and the normalized isentropic slope. The normalized isentropic slope, in turn, is directly related to the criticality parameter as $\hat{s} \sim \xi L/a$. For a spherical planet, where $L \sim a$, $\hat{s}$ scales directly with the criticality parameter. In our numerical simulations where the "planetary scale" a is varied independently of L, the normalized slope and the criticality parameter can be different. But the key point is that knowledge of the criticality parameter implies knowledge of the normalized isentropic slope, and vice versa. Notice that we assume that the width of the baroclinic zone is constrained by the size of the domain, as appropriate for our simulations and planetary atmospheres. Some idealized studies have looked at relatively sharp baroclinically forced regions, embedded in a much larger domain. In this case eddies modify the temperature gradient by setting the width of the baroclinic zone itself (e.g. Zurita-Gotor and Vallis 2009). A detailed discussion of this case is beyond the scope of this study.

Equation (20) can also be used to infer the bulk static stability, which follows by dividing both sides of the equation by $\hat{s}$:

$$\Delta_v \overline{b} \approx \frac{\Delta_h b_{\mathrm{eq}}}{\hat{s} + \hat{s}^{-1}}. \tag{21}$$

The bulk static stability, like the horizontal buoyancy contrast, can be expressed in terms of the radiative

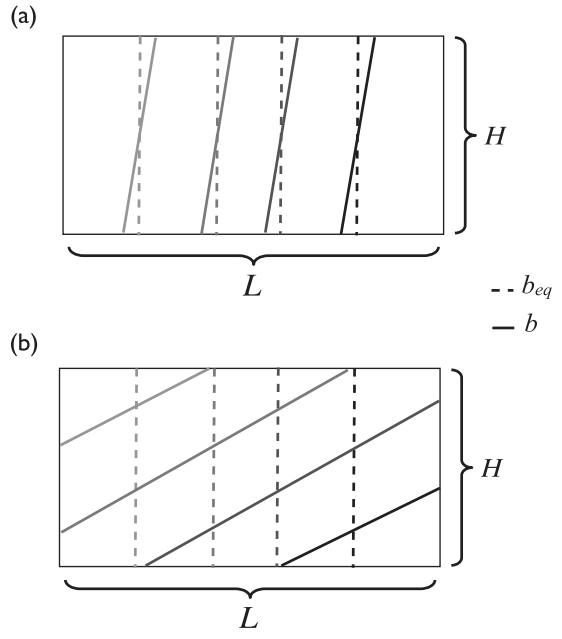

FIG. 8. Sketch of an idealized baroclinic flow. Solid lines denote mean isentropes of the equilibrated turbulent flow, while dashed lines denote the radiative equilibrium state. (a) A case where the slope of the isentropes is much steeper than the aspect ratio of the baroclinic domain: $\hat{s} \gg 1$. (b) A case where the slope of the isentropes is on the same order as the aspect ratio of the baroclinic domain: $\hat{s} \approx 1$.

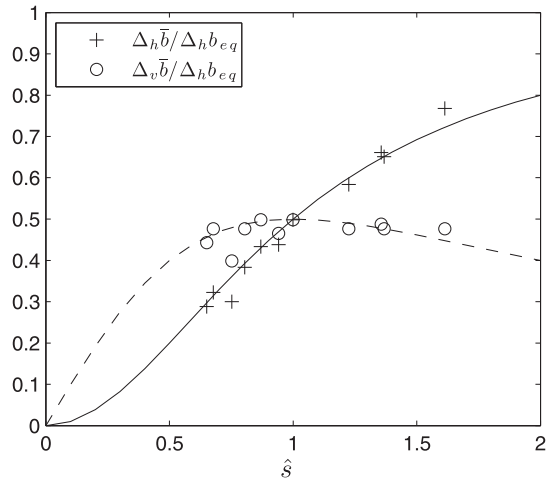

FIG. 9. Horizontal buoyancy contrast (plus signs) and bulk stability (circles), normalized by the radiative equilibrium horizontal buoyancy contrast, as a function of the normalized isentropic slope, for the series of simulations with varying f and β. The gray lines show the theoretical predictions using Eqs. (20) and (21), for the normalized horizontal buoyancy contrast (solid) and for the bulk stability (dashed). As discussed in the text, the reference scale for the width of the baroclinic zone was chosen as $L = 8000$ km to best match the numerical results.

equilibrium horizontal buoyancy contrasts and the normalized isentropic slope. For fixed isentropic slope, Eqs. (20) and (21) suggest that both the meridional buoyancy gradient and bulk static stability are directly proportional to the meridional buoyancy gradient in radiative equilibrium. Deviations from this behavior are obtained only if the isentropic slope changes, which in turn is expected if the eddy diffusivity changes [Eq. (8)].

It is worthwhile to consider the behavior of the horizontal buoyancy contrast and bulk static stability in some limit cases. In the limit of steep isentropic slopes, $\hat{s} \gg 1$, Eq. (20) suggests that $\Delta_h\overline{b} \approx \Delta_h b_{\rm eq}$: eddies tilt the isentropes only slightly from the vertical, while leaving the horizontal buoyancy contrast almost unaltered from its radiative equilibrium value (see sketch in Fig. 8a). Turbulent eddies are thus expected to modify the isentropic slope (or criticality) primarily via changes in the stratification, which to leading order becomes $\Delta_v\overline{b} \approx \hat{s}^{-1}\Delta_h b_{\rm eq}$. As shown in appendix A, this result is not altered by the presence of a vertical gradient in the radiative equilibrium profile.

For Earth's atmosphere $\hat{s} \approx \xi \approx 1$, in which case Eq. (20) predicts that the meridional buoyancy gradient is only about half of its radiative equilibrium value (see sketch in Fig. 8b). Moreover, Eq. (21) suggests that the normalized bulk static stability $\Delta_v\overline{b}/\Delta_h b_{\rm eq}$ has a maximum at $\hat{s} \approx 1$. The normalized bulk stability in this case is thus only weakly sensitive to changes in the isentropic slope, while the normalized horizontal buoyancy gradient $\Delta_h\overline{b}/\Delta_h b_{\rm eq}$ is approximately proportional to $\hat{s}$. This implies that a change in the turbulent eddies can modify the isentropic slope via a change in the horizontal buoyancy gradient, while the bulk static stability stays roughly constant. As shown in appendix A, the addition of a vertical gradient in the radiative equilibrium buoyancy contrast modifies this result only quantitatively by shifting the exact position of the maximum in $\Delta_v\overline{b}/\Delta b_{\rm eq}$.

Equations (20) and (21), together with the scaling relation for the criticality parameter in Eq. (13), fully characterize the equilibration of the thermal mean state. Notice that the scaling for the criticality parameter as formulated in Eq. (13) includes the normalized deformation radius L_d/a, which itself depends on the static stability. In appendix B we discuss how Eqs. (13) and (20) can be combined to obtain a closed expression for the normalized isentropic slope in terms of only external parameters.

b. Comparison to numerical results

We now test the predictions of the scaling relations in Eqs. (20) and (21) against numerical simulations. Figure 9 shows $\Delta_h\overline{b}/\Delta_h b_{\rm eq}$ and $\Delta_v\overline{b}/\Delta_h b_{\rm eq}$ as a function of $\hat{s}$, for the simulations in JF13a, with varying f_0 and β (see Table 1). The average bulk stability, $\Delta_v\overline{b} = H\langle\partial_z\overline{b}\rangle$, and

horizontal buoyancy gradient $\langle \partial_y \overline{b} \rangle$ are calculated as discussed in section 3b. As discussed above, some freedom exists for the exact choice of L, which is used in the computation of the horizontal buoyancy contrast $\Delta_h \overline{b} \equiv -L \langle \partial_y \overline{b} \rangle$. A good fit to the numerical simulations is obtained by choosing $L = 8000$ km. This is somewhat larger than the width of the baroclinically forced region (7000 km wide) but somewhat smaller than the full width of the domain (9000 km wide).

Figure 9 confirms the scaling relations in Eqs. (20) and (21) for the variations in the horizontal buoyancy contrast and bulk stability associated with changes in the isentropic slope. In particular, we find that changes in the slope are primarily associated with changes in the horizontal buoyancy contrast, while the bulk stability stays relatively constant. This is in agreement with Eq. (21), which predicts that the bulk stability has a maximum at a normalized slope $\hat{s} = 1$. Since $\hat{s}$ here varies only between about 0.7 and 1.6, the bulk stability stays close to this maximum value.

While the simulations with varying rotational parameters f_0 and β exhibit a large range of criticality parameters (spanning about one order of magnitude), these variations are dominantly associated with changes in the planetary scale, $a \equiv f_0/\beta$. The simulations cover only a relatively small range of normalized isentropic slopes, spanning a factor of about 2. To explore the behavior for a larger range of isentropic slopes, we look at the simulations in JF12, where changes in the criticality parameter are achieved by variations in the thermal expansion coefficients (see Table 1). Since a is held constant in these simulations, changes in the criticality parameter translate directly into similar changes in the normalized isentropic slope, $\hat{s} \sim \xi L/a$.

Figure 10 shows $\Delta_h \overline{b}/\Delta_h b_{\mathrm{eq}}$ and $\Delta_v \overline{b}/\Delta_h b_{\mathrm{eq}}$ as a function of $\hat{s}$ for the simulations in JF12. Notice that these simulations use a restoring condition to a statically unstable buoyancy profile—a generalization that we did not include in the derivation of Eqs. (20) and (21). Nevertheless, the simulations qualitatively follow the relations derived above. In particular, we observe the decrease of the bulk stability for large normalized slopes, as the horizontal buoyancy contrast asymptotically approaches its radiative equilibrium value. To quantitatively reproduce the results in these simulations, we need to include the negative stratification of the radiative equilibrium profile, which improves the fits. The generalization of Eqs. (20) and (21) to nonneutral radiative equilibrium profiles is discussed in appendix A.

The results found here for the meridional buoyancy gradient and static stability are in agreement with the numerical simulations discussed by Zurita-Gotor (2008). He analyzed changes in the meridional temperature gradient and bulk static stability, as found in a series of simulations with strongly varying radiative restoring time scales for the mean state. Consistent with our arguments, he found that changes in the criticality parameter were dominated by changes in the meridional temperature gradient for $O(1)$ criticalities and by changes in static stability for steep isentropic slopes [see Fig. 4b in Zurita-Gotor (2008)].

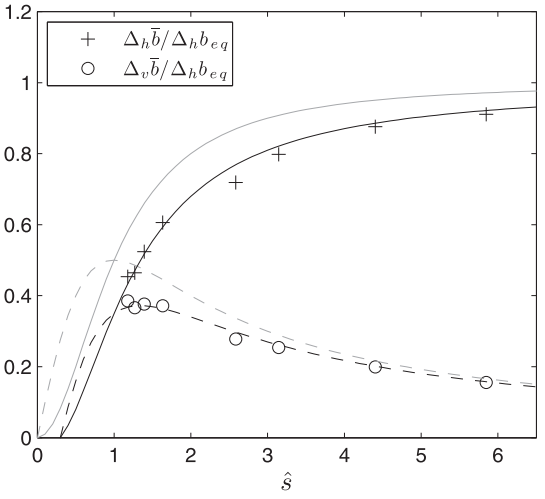

FIG. 10. As in Fig. 9, but for the simulations in JF12, with varying thermal expansion coefficients. The gray lines show the theoretical predictions using Eqs. (20) and (21), which do not consider thermal restoring to a statically unstable radiative equilibrium state. The black lines show the predictions using Eqs. (A1) and (A2), with $\Delta_v b_{\mathrm{eq}}/\Delta_h b_{\mathrm{eq}} = -0.3$ (see appendix A).

5. Conclusions

We showed that the equilibration of an idealized primitive equation model can be understood in terms of scaling relations derived from the balance between the radiative forcing and the adiabatic eddy fluxes. The scaling relations predict a weak dependence of ξ to changes in the radiative restoring, as observed in previous studies, but also show that the criticality parameter can change strongly in response to changes in other external parameters, such as the planetary size or rotation rate. This result is confirmed by a series of numerical simulations in a primitive equation, β-plane, channel model, with varying Coriolis parameters f and planetary vorticity gradients β.

To the extent that the idealized dry system considered here can be used to make inferences about Earth's atmosphere, our results suggest that changes in the criticality parameter in response to changes in the radiative forcing, as expected in past and future climate change, are likely to be small. However, if other parameters are varied, or if the forcing is varied strongly enough, the criticality parameter can become much larger than one.

The assumption that large-scale turbulence generally equilibrates planetary atmospheres to states of marginally criticality does not hold.

The criticality parameter (which implies a constraint on the isentropic slope) was further used to predict both the bulk stability and the horizontal buoyancy gradient. We derived scaling relations for the equator-to-pole temperature gradient and bulk stability as a function of the isentropic slope and the radiative equilibrium temperature profile. Both are to first order proportional to the radiative equilibrium horizontal temperature gradient. In addition, the horizontal temperature gradient increases toward its radiative equilibrium value with increasing isentropic slopes. The bulk stability instead is only weakly sensitive to the isentropic slope for slopes typically found in Earth's atmosphere, and thus it is almost directly proportional to the radiative equilibrium equator-to-pole temperature gradient. Combining the scaling relation for the criticality parameter with those for the meridional temperature gradient and static stability allows us to fully characterize the atmospheric mean state as a function of external parameters.

Our results have interesting implications for the understanding of planetary climates, as well as past and future climates on Earth. They extend the concept of climate sensitivity beyond the zero-dimensional picture of the global mean temperature response to global mean changes in the forcing. For instance, we find that a change in the radiative equilibrium equator-to-pole temperature gradient is associated with an approximately proportional change in the bulk static stability. The static stability in turn has a strong effect on the surface temperature because it sets the temperature difference between the surface and the effective emission level. Yet, energy balance models discussed in the existing literature typically assume a constant static stability (e.g., Huybers and Tziperman 2008; Rose and Marshall 2009). Our results will hopefully motivate a more thorough consideration of the role of changes in the static stability for the dynamics and thermodynamics of the atmosphere.

Acknowledgments. We want to thank Paul O'Gorman, Alan Plumb, and Isaac Held for helpful comments and discussions. This work was supported through NSF Award OCE-0849233.

APPENDIX A

The Meridional Buoyancy Gradient and Static Stability in the Presence of Finite $\Delta_v b_{eq}$

We here want to generalize the results for the horizontal buoyancy contrast and bulk static stability in Eqs. (20) and (21) to account for a radiative restoring, which acts toward a stratification that is not statically neutral; that is, $\Delta_v b_{eq} \sim H\langle \partial_z b_{eq} \rangle \neq 0$. The arguably most realistic representation of the real atmosphere is given by a radiative restoring to a statically unstable state; that is, $\Delta_v b_{eq} < 0$. The case where $\Delta_v b_{eq} > 0$ is primarily of theoretical interest since it allows us to recover the QG limit, when the stratification converges toward its radiative equilibrium value (see also Zurita-Gotor and Vallis 2010).

Rearrangement of Eq. (19) generally yields that

$$\Delta_h \overline{b} \approx \frac{\Delta_h b_{eq} + \hat{s}^{-1} \Delta_v b_{eq}}{1 + \hat{s}^{-2}}. \tag{A1}$$

Using that $\Delta_v \overline{b} = \hat{s}^{-1} \Delta_h \overline{b}$, we directly find that

$$\Delta_v \overline{b} \approx \frac{\Delta_h b_{eq} + \hat{s}^{-1} \Delta_v b_{eq}}{\hat{s} + \hat{s}^{-1}}. \tag{A2}$$

As in Eqs. (20) and (21), we find that both the horizontal buoyancy contrast and the bulk stability can be expressed as a function of the radiative equilibrium buoyancy profile and the normalized isentropic slope. However, both the horizontal buoyancy contrast and the stratification of the radiative equilibrium profile now influence the resulting mean state.

As in the simplified Eqs. (20) and (21), the normalized horizontal buoyancy contrast approaches its radiative equilibrium value; that is, $\Delta_h \overline{b} \approx \Delta_h b_{eq}$, in the limit that $\hat{s} \gg 1$. Any further increase in the isentropic slope in this limit is accomplished primarily by a further reduction of the normalized stratification $\Delta_v \overline{b} / \Delta_h b_{eq}$. Also as in Eqs. (20) and (21), the normalized stratification $\Delta_v \overline{b} / \Delta_h b_{eq}$ has a maximum at an $O(1)$ normalized isentropic slope, as long as $|\Delta_v b_{eq}| \lesssim |\Delta_h b_{eq}|$. The exact location of this maximum depends on the exact value of $\Delta_v b_{eq} / \Delta_h b_{eq}$. For a radiative restoring acting to a statically unstable profile (i.e., $\Delta_v b_{eq} < 0$), the maximum in $\Delta_v \overline{b} / \Delta_h b_{eq}$ is shifted to larger values of $\hat{s}$. The effect of adding a moderate radiative destabilization, $\Delta_v b_{eq} = -0.3 \Delta_h b_{eq}$, is shown in Fig. 10.

Notice that Eq. (A2) would predict a negative stratification if $\Delta_v b_{eq} < -\Delta_h b_{eq} \hat{s}$. In the case of restoring to a statically unstable mean state [Eq. (A2)] thus does not have a physical solution for normalized isentropic slopes weaker than $-\Delta_v b_{eq} / \Delta_h b_{eq}$. This suggests that, in the limit of very effective adiabatic mixing, the mean state equilibrates to $\hat{s} = -\Delta_v b_{eq} / \Delta_h b_{eq}$, with both $\Delta_v \overline{b}, \Delta_h \overline{b} \to 0$. This result can also be obtained directly from Eq. (19), taking the limit where $\Delta_h \overline{b} \ll \Delta_h b_{eq}$ and $\Delta_v \overline{b} \ll \Delta_v b_{eq}$. In how far the scaling argument in Eq. (A2) holds in such a limit is, however, yet to be tested. It is also possible that a system in this limit equilibrates to a state that is strongly

inhomogeneous over the domain, such that "characteristic" isentropic slopes, buoyancy gradients, and stratifications, as defined here, become meaningless and the presented scaling arguments break down. Further, it may be questioned in how far the assumption of adiabatic eddy fluxes is appropriate in such a limit.[A1]

The QG limit is retained if the isentropic slope is weak (i.e., $\hat{s} \ll 1$) and the restoring acts to a statically stable state, in which $\Delta_v b_{\mathrm{eq}}/\Delta_h b_{\mathrm{eq}} \gtrsim 1$. In this limit, Eq. (A2) reduces to $\Delta_v \overline{b} = \Delta_v b_{\mathrm{eq}}$, and changes in the isentropic slope are solely due to changes in the meridional buoyancy gradient. Notice, however, that this limit is likely to be of little relevance for the real atmosphere.[A2]

Notice that the radiative restoring profile used in the simulations of JF12 cannot trivially be characterized by a single equilibrium stratification $\partial_z b_{\mathrm{eq}}$, as the latter varies strongly (and even changes sign) over the depth of the troposphere. For Fig. 10, we chose $\Delta_v b_{\mathrm{eq}} = -0.3\Delta_h b_{\mathrm{eq}}$, which produces a good fit to the data, and subjectively represents an adequate linear fit to the horizontal mean restoring profile. The radiative equilibrium horizontal temperature contrast, $\Delta_h \theta_{\mathrm{eq}} = \alpha^{-1}\Delta_h b_{\mathrm{eq}}$, was chosen similar to the simulations with varying f_0 and β, which is an obvious choice, as they share the same radiative convective equilibrium solution.

APPENDIX B

Predicting the Normalized Isentropic Slope from External Parameters

In section 3 we derived a scaling relation expressing the criticality parameter in terms of the normalized radiative restoring time scale τf and the normalized deformation radius L_d/a. While this represents a closed relation for the mean state, it does not quite give us a fully predictive scaling for the criticality parameter and thus isentropic slope in terms of only external parameters, since $L_d \propto \sqrt{\partial_z \overline{b}}$ is itself a mean-state variable, determined by the turbulent equilibration. For simulations with varying rotational parameters, f and β, it was found that changes in the static stability are negligible, such that the full scaling relation for the criticality parameter can to first order be reduced to its dependence on the externally prescribed parameters f and β. However, the weak variation in the static stability for the considered set of simulations was itself a result of the numerical simulations and was predicted only by the additional scaling relation for the bulk static stability discussed in section 4.

In general we can combine the scaling relations for the criticality parameter in section 3 with the one for the bulk static stability discussed in section 4 to derive expressions for the isentropic slope, and thus [with Eqs. (20) and (21)] for the meridional temperature gradient and static stability, in terms of only external parameters.

For simplicity we again want to assume radiative restoring to a statically neutral buoyancy profile. Equation (13) can be used to obtain a scaling relation for the isentropic slope as

$$\hat{s} \sim \frac{L}{a}(f\tau)^{-1/5}\left(\frac{\Delta_v \overline{b} H}{f^2 a^2}\right)^{-3/10}. \tag{B1}$$

Substituting Eq. (21) for $\Delta_v \overline{b}$ in Eq. (B1) and rearranging terms yields

$$\hat{s}(\hat{s} + \hat{s}^{-1})^{-3/10} = \gamma, \tag{B2}$$

where γ is a nondimensional parameter that can be expressed as

$$\gamma = c\frac{L}{a}(f\tau)^{-1/5}\left(\frac{\Delta_h b_{\mathrm{eq}} H}{f^2 a^2}\right)^{-3/10} = c\frac{L\beta^{2/5}}{\tau^{1/5}\Delta_h b_{\mathrm{eq}}^{3/10} H^{3/10}}, \tag{B3}$$

with c an $O(1)$ constant (found to be about 0.9 in our simulations).

Equation (B2) implies that $\hat{s} = f(\gamma)$, where the function f is obtained by inversion of Eq. (B2). Together with Eqs. (20) and (21), this suggests that changes in the thermal mean state of the system are entirely determined by changes in γ in Eq. (B3). For a more detailed discussion of this relation, as well as the derivation of a generalized relation for the case of nonneutral radiative restoring profiles, the reader is referred to Jansen (2012).

Finally, it should be noted that we here assumed the tropopause height H to be an external parameter. While this is reasonable for the simulations discussed here, where H is strongly constrained by the radiative restoring profile, other forcing profiles may allow H to change strongly (e.g., Zurita-Gotor and Vallis 2011). In this case, Eqs. (B2) and (B3) would have to be combined

[A1] Notice that, even if eddies are adiabatic in the sense that $\overline{b'Q'} = 0$, the applied assumption that $\overline{w'b'}/\overline{v'b'} = s$ still requires that the advection of buoyancy variance (primarily associated with the triple correlation term in the variance budget) is negligible (e.g., Cerovečki et al. 2009 and references therein).

[A2] One possible way to argue that this limit could become relevant for the atmosphere is to consider latent heat release as an external forcing in a warm, moist, climate. One might argue that the latent heat release due to moist convection here acts as a restoring to a dry statically stable state. In how far dry dynamics are at all relevant in such a case, and in how far latent heat release can be reasonably thought of as an external diabatic forcing, however, remains questionable.

with an additional constraint on the tropopause height to obtain a truly predictive equation. Theoretically such a constraint should be given by a ''matching condition'' between the dynamically controlled tropospheric temperature profile and the radiative equilibrium temperature profile above (e.g., Held 1982). In practice, combining such a constraint with the relations derived here might, however, be algebraically rather daunting. It also remains unclear in how far strong changes in the tropopause height are important in the equilibration of Earth's atmosphere. When considering an ideal gas atmosphere, the relevant ''depth'' scale entering into the criticality parameter is the pressure contrast between the surface and the tropopause (e.g., Schneider 2004). In pressure coordinates, the radiative equilibrium temperature profile in Earth's atmosphere does increase quite sharply above the troposphere, suggesting that changes in the depth of the troposphere may indeed be negligible.

REFERENCES

Cerovečki, I., R. A. Plumb, and W. Heres, 2009: Eddy transport and mixing in a wind and buoyancy-driven jet on the sphere. *J. Phys. Oceanogr.,* **39,** 1133–1149.

Gent, P. R., and J. C. McWilliams, 1990: Isopycnal mixing in ocean circulation models. *J. Phys. Oceanogr.,* **20,** 150–155.

——, J. Willebrand, T. J. McDougall, and J. C. McWilliams, 1995: Parameterizing eddy-induced tracer transports in ocean circulation models. *J. Phys. Oceanogr.,* **25,** 463–474.

Held, I. M., 1978: The vertical scale of an unstable baroclinic wave and its importance for eddy heat flux parameterizations. *J. Atmos. Sci.,* **35,** 572–576.

——, 1982: On the height of the tropopause and the static stability of the troposphere. *J. Atmos. Sci.,* **39,** 412–417.

——, 2007: Progress and problems in large-scale atmospheric dynamics. *The Global Circulation of the Atmosphere,* T. Schneider and A. H. Sobel, Eds., Princeton University Press, 1–21.

——, and M. J. Suarez, 1994: A proposal for the intercomparison of the dynamical cores of atmospheric general circulation models. *Bull. Amer. Meteor. Soc.,* **75,** 1825–1830.

——, and V. D. Larichev, 1996: A scaling theory for horizontally homogeneous baroclinically unstable flow on a beta plane. *J. Atmos. Sci.,* **53,** 946–952.

Huybers, P., and E. Tziperman, 2008: Integrated summer insolation forcing and 40,000-year glacial cycles: The perspective from an ice-sheet/energy-balance model. *Paleoceanography,* **23,** PA1208, doi:10.1029/2007PA001463.

Jansen, M., 2012: Equilibration of a dry atmosphere by geostrophic turbulence. Ph.D. dissertation, Massachusetts Institute of Technology, 187 pp.

——, and R. Ferrari, 2012: Macroturbulent equilibration in a thermally forced primitive equation system. *J. Atmos. Sci.,* **69,** 695–713.

——, and ——, 2013: The vertical structure of the eddy diffusivity and the equilibration of the extratropical atmosphere. *J. Atmos. Sci.,* **70,** 1456–1469.

Lapeyre, G., and I. M. Held, 2003: Diffusivity, kinetic energy dissipation, and closure theories for the poleward eddy heat flux. *J. Atmos. Sci.,* **60,** 2907–2916.

Marshall, J., C. Hill, L. Perelman, and A. Adcroft, 1997: Hydrostatic, quasi-hydrostatic, and nonhydrostatic ocean modeling. *J. Geophys. Res.,* **102** (C3), 5753–5766.

Plumb, R., and R. Ferrari, 2005: Transformed Eulerian-mean theory. Part I: Nonquasigeostrophic theory for eddies on a zonal-mean flow. *J. Phys. Oceanogr.,* **35,** 165–174.

Rose, B., and J. Marshall, 2009: Ocean heat transport, sea ice, and multiple climate states: Insights from energy balance models. *J. Atmos. Sci.,* **66,** 2828–2843.

Schneider, T., 2004: The tropopause and the thermal stratification in the extratropics of a dry atmosphere. *J. Atmos. Sci.,* **61,** 1317–1340.

——, and C. C. Walker, 2006: Self-organization of atmospheric macroturbulence into critical states of weak nonlinear eddy–eddy interactions. *J. Atmos. Sci.,* **63,** 1569–1586.

Stone, P. H., 1978: Baroclinic adjustment. *J. Atmos. Sci.,* **35,** 561–571.

Thompson, A., and W. Young, 2007: Two-layer baroclinic eddy heat fluxes: Zonal flows and energy balance. *J. Atmos. Sci.,* **64,** 3214–3231.

Vallis, G. K., 2006: *Atmospheric and Oceanic Fluid Dynamics.* Cambridge University Press, 745 pp.

Zurita-Gotor, P., 2008: The sensitivity of the isentropic slope in a primitive equation dry model. *J. Atmos. Sci.,* **65,** 43–65.

——, and G. K. Vallis, 2009: Equilibration of baroclinic turbulence in primitive-equation and quasi-geostrophic models. *J. Atmos. Sci.,* **66,** 837–863.

——, and ——, 2010: Circulation sensitivity to heating in a simple model of baroclinic turbulence. *J. Atmos. Sci.,* **67,** 1543–1558.

——, and ——, 2011: Dynamics of midlatitude tropopause height in an idealized model. *J. Atmos. Sci.,* **68,** 823–838.